Ann Nucl Med (2013) 27:271–278
DOI 10.1007/s12149-012-0681-5

ORIGINAL ARTICLE

Appropriate collimators in a small animal SPECT scanner with CZT detector

Yusuke Higaki · Masato Kobayashi · Tomoya Uehara · Hirofumi Hanaoka · Yasushi Arano · Keiichi Kawai

Received: 31 October 2012 / Accepted: 26 December 2012 / Published online: 4 January 2013

Abstract
Objective Almost all small animal SPECT is performed with pinhole collimators (PH), including single-PH (SPH) and multi-PH (MPH). In the clinical study, not only PH but also parallel-hole collimator (PAH) is often used in planar and SPECT imaging. However, there have been no comparative studies on image quality with various collimators on the small animal imaging. This study compared the basic characteristics of PH and PAH in small animal imaging.
Methods Performance of planar and SPECT images was evaluated using $^{99m}TcO_4^-$ and SPH, MPH and PAH with low energy and high resolution on the SPECT/CT scanner FX3200. We measured sensitivity, resolution, concentration linearity and uniformity. Planar imaging of mice with ^{99m}Tc-labeled mercaptoacetyltriglycine (^{99m}Tc-MAG_3) was performed using SPH and PAH. SPECT imaging with ^{99m}Tc-methylene diphosphonate (^{99m}Tc-MDP) was performed using all collimators.
Results With SPH, MPH and PAH, sensitivity was 43.5, 211.2 and 926.5 cps/MBq, respectively, and spatial resolution was 0.60/0.56, non/0.96, 5.20/5.34 mm full-width half maximum (planar/SPECT), respectively. There were marked correlations between the radioactivity counts on images and radioactivity with all collimators. Values of % standard deviation on planar imaging showed small differences between the SPH and PAH, while the values were the smallest on SPECT imaging with MPH. On imaging of mice, SPH yielded high-quality ^{99m}Tc-MAG_3-planar images when compared with PAH. MPH yielded sharper ^{99m}Tc-MDP-SPECT images than SPH and PAH.
Conclusions The characteristics of PH and PAH differed on small animal imaging. Although sensitivity was higher with PAH, PH showed higher resolution. Among the PH collimators, SPH was more appropriate for planar imaging, and MPH was more suitable for SPECT imaging in a small animal imaging scanner with CZT detector.

Keywords Small animal imaging · Planar imaging · SPECT imaging · Pinhole collimator · Parallel-hole collimator

Y. Higaki · M. Kobayashi (✉) · K. Kawai
Graduate School of Health Sciences, College of Medical, Pharmaceutical and Health Sciences, Kanazawa University, 5-11-80, Kodatsuno, Kanazawa 920-0942, Japan
e-mail: kobayasi@mhs.mp.kanazawa-u.ac.jp

Y. Higaki · T. Uehara · H. Hanaoka · Y. Arano
Graduate School of Pharmaceutical Sciences, Chiba University, 1-8-1, Inohana, Chuo-ku, Chiba 260-8675, Japan

K. Kawai
Biomedical Imaging Research Center, University of Fukui, Fukui, Japan

Introduction

Single photon emission computed tomography (SPECT) for small animal imaging is a useful molecular imaging technique for tracer development and therapy evaluation, as well as for pathophysiological investigations, in small animals [1–3]. In current SPECT scanners, cadmium zinc telluride (CZT) semiconductor detectors have been applied to improve energy and spatial resolution [4–8], as compared with sodium iodide (NaI) scintillation detectors, which were used in conventional SPECT scanners [9–19]. Planar and SPECT projection data are acquired using various collimators in clinical settings. Almost all small animal SPECT is performed with pinhole collimators (PH), including single-PH (SPH) [8, 12–17] and multi-PH (MPH)

[6, 8–10, 15], as these collimators will provide good resolution for small objects when compared with parallel hole collimators (PAH), which are more commonly used in clinical settings [20]. Although we have to select appropriate collimator to obtain high-quality images and accurate analysis results, there have been no comparative studies on image quality with various collimators in small animal imaging.

In this study, we compared the performance and image quality of SPH, MPH and PAH in small animal scanner with CZT detector. Performance was evaluated using point, line and planar sources, and Derenzo phantoms. Planar and SPECT images were obtained using ^{99m}Tc-mercaptoacetyltriglycine (^{99m}Tc-MAG$_3$) and ^{99m}Tc-methylene diphosphonate (^{99m}Tc-MDP), respectively.

Materials and methods

System description

We used the FX-3200 (Gamma Media-Ideas Inc., CA, USA) as a small animal SPECT/CT scanner (Table 1). The FX-3200 has four detectors with a cadmium zinc telluride (CZT) semiconductor (20.5 × 15.5 × 9.0 cm). Three types of collimator could be attached: (1) SPH, single pinhole, focal-length 90 mm; (2) MPH, five pinhole, focal-length 75 mm; and (3) PAH with low energy and high resolution. Radius of rotation (ROR) is from 15 to 175 mm, and field of view (FOV) is a maximum of 120 mm, while detectable energy ranges from 20 to 300 keV. All imaging data were acquired at a matrix size of 80 × 80.

Sensitivity

A 3.7 MBq $^{99m}TcO_4^-$ point source was placed in the center of the FOV, and planar and SPECT data were acquired for 10 min. Distances between the phantom and each detector were reduced as far as possible. An assembly of 4 detectors with SPH and PAH was used to obtain planar imaging data. SPECT data were acquired using a circular orbit with step-and-shoot acquisition at 6° intervals over 360° for all collimators.

Table 1 Features of collimators on SPECT/CT scanner FX3200

Composition	Collimators		
	SPH	MPH	PAH
Material	Tungsten	Tungsten	Tungsten and antimony
Number of pinholes	1	5	10000
Pinhole diameter (mm)	0.5	0.5	1.22
Minimum FOV for animal imaging (mm)	26.7	46.3	120
Focal length (mm)	90	75	–

SPH single-pinhole collimator, *MPH* multi-pinhole collimator, *PAH* parallel hole collimator for low energy, high resolution, *FOV* field of view, *ROR* radius of rotation

Spatial resolution and SPECT resolution with Derenzo phantom

A glass capillary with an internal diameter of 0.5 mm containing about 3.7 MBq $^{99m}TcO_4^-$ was used as a line source. The positioning and acquisition method was the same as for sensitivity measurement. Spatial resolution was obtained using full-width half maximum (FWHM) and full-width tenth maximum (FWTM). SPECT resolution was also obtained using a Derenzo phantom (K.K.K. Nikoh Co., Shizuoka, Japan) made from acryl with four types of rod (0.5, 0.8, 1.0 and 1.2 mm in diameter) (Fig. 1d). A total of 74 MBq $^{99m}TcO_4^-$ was injected into the phantom, which was then acquired using all collimators.

Concentration linearity

The positioning and acquisition method was the same as for sensitivity and resolution measurement for each collimator. Planar and SPECT data were acquired at various time points and radioactivity levels (1.0, 2.0, 3.7, 7.4, 11.1, 14.8, 18.5, 27.8, 37.0, 74.0, 111, 148 and 185 MBq) using a planar source and cylindrical phantom (300 ml), respectively.

Uniformity

A planar source with 37 MBq $^{99m}TcO_4^-$ and a cylindrical phantom including 185 MBq $^{99m}TcO_4^-$ were placed in the center of the FOV. Planar and SPECT data were acquired for 10 and 30 min, respectively. We calculated the % standard deviation (%STD) in the regions of interest (ROI).

Planar imaging of ^{99m}Tc-MAG$_3$

Animal studies were approved by the Animal Care Committee at Chiba University and were conducted in accordance with international standards for animal welfare and institutional guidelines. Adequate measures were taken to minimize pain and discomfort. Five normal male ddy mice (29–33 g) from Japan SLC Inc. (Hamamatsu, Japan) were housed for 1 week under a 12-h light/12-h dark cycle with free access to food and water. Mice were fasted with no food overnight with water supplied ad libitum before SPECT experiments.

Five mice were anesthetized with 1.2–1.5 % isoflurane (Abbot Laboratories, Illinois, USA). A PE-10 catheter was inserted into the femoral artery for blood, and the femoral

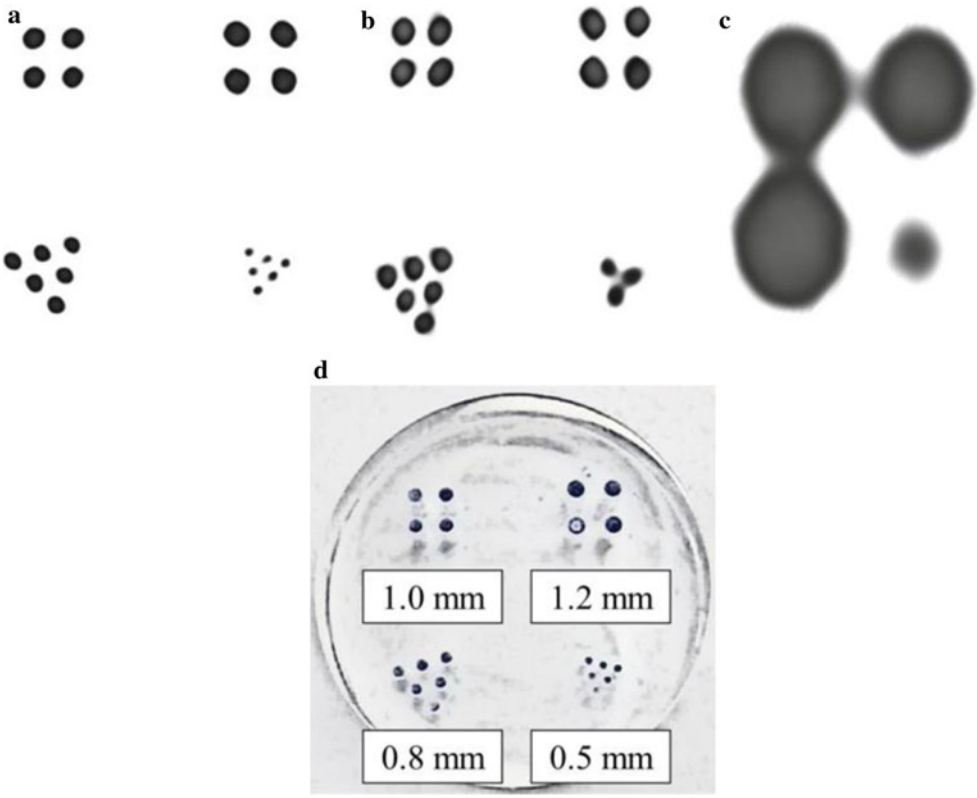

Fig. 1 SPECT imaging with the Derenzo phantom. SPECT images of phantoms were obtained after 20 min with 74 MBq $^{99m}TcO_4^-$ using all collimators. Image data were acquired using SPH (**a**) and MPH (**b**), followed by reconstruction using the 3D-OSEM algorithm (4 subsets and 20 iterations), or PAH (**c**), followed by reconstruction using a filtered back-projection algorithm. The Derenzo phantom had four rods (0.5, 0.8, 1.0 and 1.2 mm in diameter) (**d**)

vein for ^{99m}Tc-MAG$_3$ (Fujifilm RI Pharma Co., Tokyo, Japan) administration. Imaging data were acquired with the dynamic planar protocol using the small animal SPECT/CT scanner FX-3200. Mice were placed in the supine position on the scanner bed, and limbs were fixed using surgical tape. The orientation of the renal position was determined using a laser beam and CT imaging on the scanner. After setting ROR to be maximally close to mice, dynamic scans (2 s × 30 frames, 5 s × 48 frames and 30 s × 30 frames) with SPH were started with an intravenous bolus administration of about 15 MBq ^{99m}Tc-MAG$_3$ using an microinjection pump CFX1010 (ISIS, Osaka, Japan) for 15–20 s. On the next day, the same mice were used for experiments using the same scanning protocol with PAH and ROR being set maximally close to mice. For 2 further days, the same mice were evaluated using 74 MBq ^{99m}Tc-MAG$_3$ under the same experimental protocol as with 15 MBq ^{99m}Tc-MAG$_3$. Voxel sizes were 0.53 × 0.53 × 0.37 with SPH and 0.70 × 0.70 × 0.50 mm with PAH, respectively. Regions of interest were placed over whole kidneys in ^{99m}Tc-MAG$_3$ images.

SPECT imaging of ^{99m}Tc-MDP

Three normal ddy mice were injected with 74 MBq of ^{99m}Tc-MDP (Fujifilm RI Pharma Co., Tokyo, Japan) via the tail vein. Positioning and scanning preparation were the same as with ^{99m}Tc-MAG$_3$. ROR was set to be maximally close to mice for SPECT imaging using each collimator. At 30 min after injection, whole-body SPECT imaging data were started for 30 min using each collimator. Voxel sizes were 0.53 × 0.53 × 0.37 mm with SPH, 0.43 × 0.43 × 0.31 mm with MPH and 0.70 × 0.70 × 0.50 mm with PAH.

Reconstruction methods and image analyses

Planar and SPECT imaging data with PAH were reconstructed using a filtered back-projection algorithm with a ramp filter, which is a reconstruction filter. For SPECT imaging data with SPH and MPH, a 3D-ordered subset expectation maximization (3D-OSEM) algorithm was applied using 4 subsets and 20 iterations in FLEX-RECON software. In the all planar and SPECT imaging, pre and post-filters were not used. Imaging data were analyzed using amide's medical imaging data examiner.

Results

Sensitivity

Sensitivity data are summarized in Table 2. On planar imaging, sensitivity with PAH was higher than that with SPH. On SPECT imaging, the highest sensitivity was achieved using PAH, followed by MPH and SPH.

Table 2 Sensitivity of collimators on planar and SPECT imaging

Collimators	Sensitivity (cps/MBq)	
	Planar	SPECT
SPH	4.0	43.5
MPH	Non	211.2
PAH	239.1	926.5

SPH single-pinhole collimator, *MPH* multi-pinhole collimator, *PAH* parallel collimator for low energy, high resolution

Spatial resolution and SPECT resolution with Derenzo phantom

Spatial resolution data are shown in Table 3. Resolution on planar images was 0.60 mm with SPH and 5.20 mm with PAH. On SPECT imaging, resolution was 0.56, 0.96 and 5.34 mm using SPH, MPH and PAH, respectively. On SPECT with the Derenzo phantom, SPH provided the best quality images (Fig. 1).

Concentration linearity

Concentration linearity is shown in Fig. 2. Correlations between radioactivity and radioactive counts for planar and SPECT images showed marked linearity (about 1.0) for all collimators.

Uniformity

Uniformity data are shown in Table 4. The %STDs on planar imaging were 11.3 with SPH and 9.3 with PAH. On SPECT imaging, the %STDs were 20.5, 9.2 and 16.8 using SPH, MPH and PAH, respectively.

Planar imaging of ^{99m}Tc-MAG$_3$

On ^{99m}Tc-MAG$_3$ images, cortexes of the kidney with SPH were much clearer than those with PAH (Fig. 3). Time activity curves (TACs) for the kidney with ^{99m}Tc-MAG$_3$ are shown in Fig. 4. TACs with SPA and PAH showed clear peaks for radioactivity and smooth washout when 74 MBq of ^{99m}Tc-MAG$_3$ was injected into mice. When 15 MBq of ^{99m}Tc-MAG$_3$ was used, TACs with PAH showed an ideal radioactivity peak and washout, while TACs with SPH had an unclear peak and much dispersion.

SPECT imaging of ^{99m}Tc-MDP

^{99m}Tc-MDP images with SPH and MPH were good when compared to those with PAH (Fig. 5). In particular, separation of the spine was clearest in the ^{99m}Tc-MDP images with MPH.

Table 3 Spatial resolution of collimators on planar and SPECT imaging

Collimators	FWHM/FWTM (mm)	
	Planar	SPECT
SPH	0.60/1.09	0.56/1.03
MPH	Non/1.53	0.96/1.75
PAH	5.20/9.49	5.34/9.74

FWHM full-width half maximum, *FWTM* full-width tenth maximum, *SPH* single-pinhole collimator, *MPH* multi-pinhole collimator, *PAH* parallel collimator for low energy, high resolution

Discussion

In this study, we evaluated the performance of the SPECT scanner with various collimators, and assessed planar and SPECT imagings with mice in order to confirm the suitability of these collimators for animal imaging. There are few commercially available small animal imaging scanners that are able to perform both planar and SPECT imagings using CZT detector with various collimators except our imaging scanner. As shown in Table 2, sensitivity with PAH on planar imaging was about 60-fold higher than that with SPH. These results are important because the sensitivity has not previously been reported on the SPECT scanner with CZT detector. In other scanners, the sensitivity of planar imaging using the Inveon SPECT scanner with NaI detector (Siemens Medical Solutions, TN, USA) was about 35 cps/MBq with SPH [12]. Thus, the sensitivity on the Inveon SPECT scanner was about 8.8-fold higher than that on our scanner because the imaging scanner with NaI detector has higher sensitivity than that with CZT detector. On SPECT imaging, sensitivity with MPH was about fivefold higher than that with SPH, while PAH yielded about 21-fold higher sensitivity than SPH. The sensitivity was lower than with other scanners with NaI detector [10, 12, 14, 15, 17].

In our scanner, the resolution of planar and SPECT imagings with SPH and MPH was 1 mm or less, while PAH provided about 5 mm (Table 3). In other scanners, SPH provided 0.6–1.4 mm FWHM with NaI detector [12–15] and 1.0 mm FWHM with CZT detector [8]. MPH produced about 1.2 mm FWHM with NaI detector [15] and 1.2–1.4 mm with CZT detector [6, 8]. PAH yielded about 8 mm FWHM with NaI detector [13]. Thus, our results of PH were great compared with those of PAH and other scanners. On SPECT imaging using the Derenzo phantom, SPECT resolutions with SPH and MPH were 0.5 and 0.8 mm, respectively, and PAH could not display 1.2 mm (Fig. 1). In other scanners, SPECT resolutions with Derenzo phantom were about 1.0 mm FWHM using CZT detector with MPH [6] and 0.35–0.5 mm FWHM using NaI detector

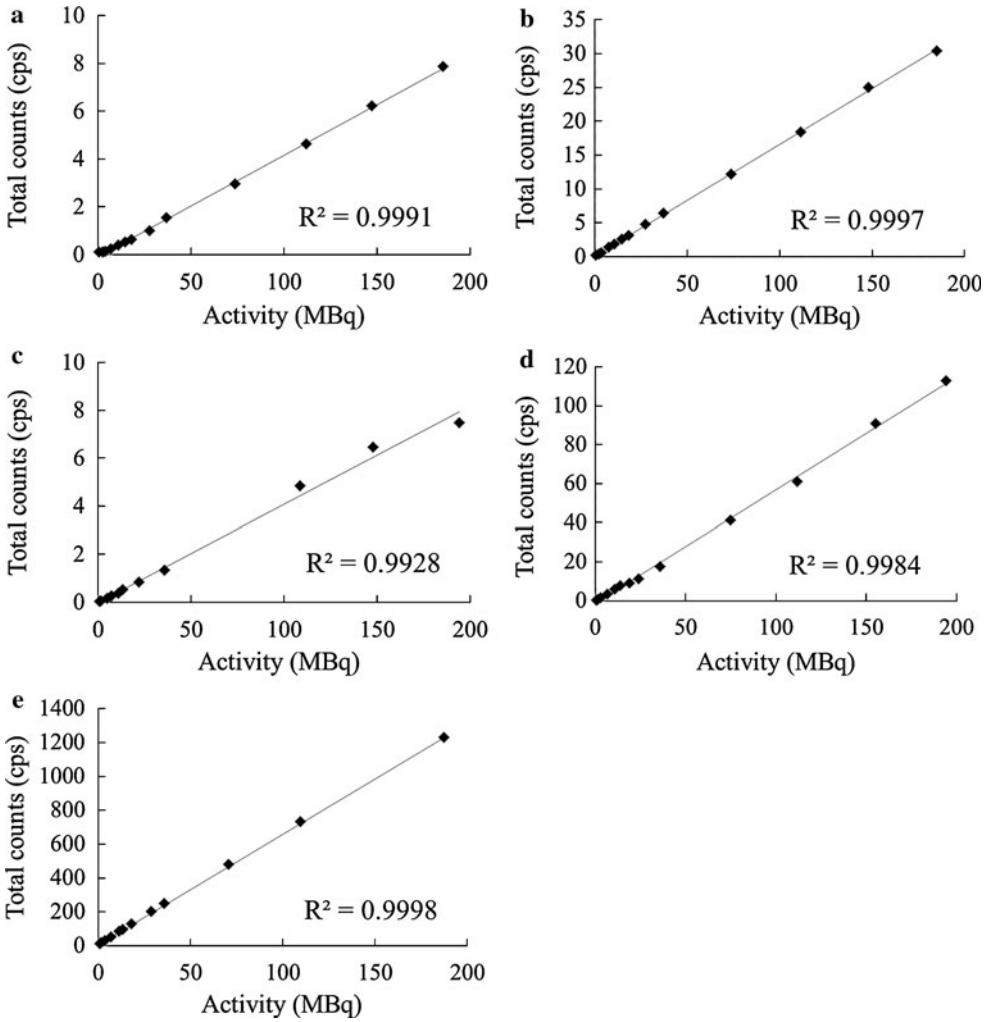

Fig. 2 Concentration linearity was marked on planar imaging with SPH (**a**) and PAH (**b**). On SPECT images, linearity also was marked with SPH (**c**), MPH (**d**) and PAH (**e**)

Table 4 Uniformity of collimators on planar and SPECT imaging

Collimators	%STD	
	Planar	SPECT
SPH	11.3	20.5
MPH	Non	9.2
PAH	9.3	16.8

%STD % standard deviation, *SPH* single-pinhole collimator, *MPH* multi-pinhole collimator, *PAH* parallel collimator for low energy, high resolution

with MPH [9, 10]. Our results were little changed compared with other scanners.

For concentration linearity, there were marked correlations between radioactivity from low to high and radioactive counts on planar and SPECT images, regardless of collimator type (Fig. 2). With regard to uniformity, %STD values on planar imaging showed small differences between the SPH and PAH, while the values were the smallest on SPECT imaging with MPH (Table 4). On other scanners, %STDs in the SPECT imaging showed small values when compared with our scanners [12], as no pre and post-filters were used for our SPECT images. Therefore, we further confirmed that SPH, MPH and PAH produced different performances although Mok et al. [8] examined the differences in performance between SPH and MPH in other scanners.

On planar imaging with ^{99m}Tc-MAG$_3$, ideal TACs were obtained using SPH (Fig. 3c) and PAH (Fig. 3d) when 74 MBq of ^{99m}Tc-MAG$_3$ was injected into mice. When using SPH, renal cortices and calices were clearly distinguished (Fig. 3a, c). Although mouse imaging using about 37 MBq ^{99m}Tc-MAG$_3$ was reported in previous studies, clear renal images were not obtained, as gamma camera and clinical scanner using NaI detector with PAH were applied for ^{99m}Tc-MAG$_3$ imaging with mice [18, 19]. To our knowledge, this is the first study to obtain high-resolution images of the kidney using mice injected with 74 MBq ^{99m}Tc-MAG$_3$ on small animal SPECT imaging. However, on mouse imaging with 15 MBq ^{99m}Tc-MAG$_3$, the radioactive peak on TAC was not clear, and the

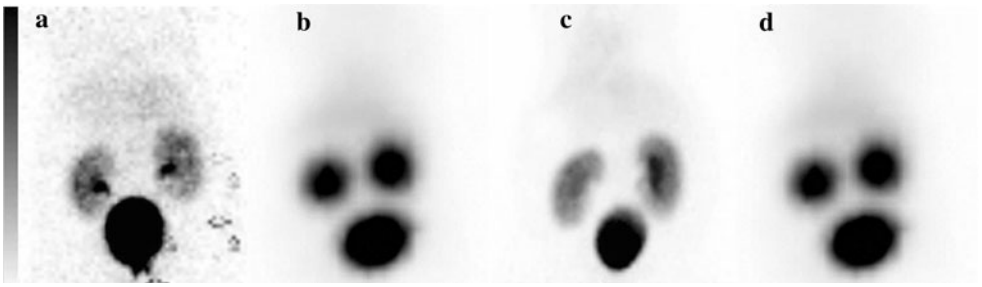

Fig. 3 Planar images with ^{99m}Tc-MAG$_3$ using mice. Planar images of mice were obtained for 20 min with 15 MBq ^{99m}Tc-MAG$_3$ using SPH (**a**) and PAH (**b**). After decay of radioactivity, 74 MBq ^{99m}Tc-MAG$_3$ was injected into the mice and planar images were obtained using SPH (**c**) and PAH (**d**). Renal cortices were much clearer on ^{99m}Tc-MAG$_3$ imaging with SPH

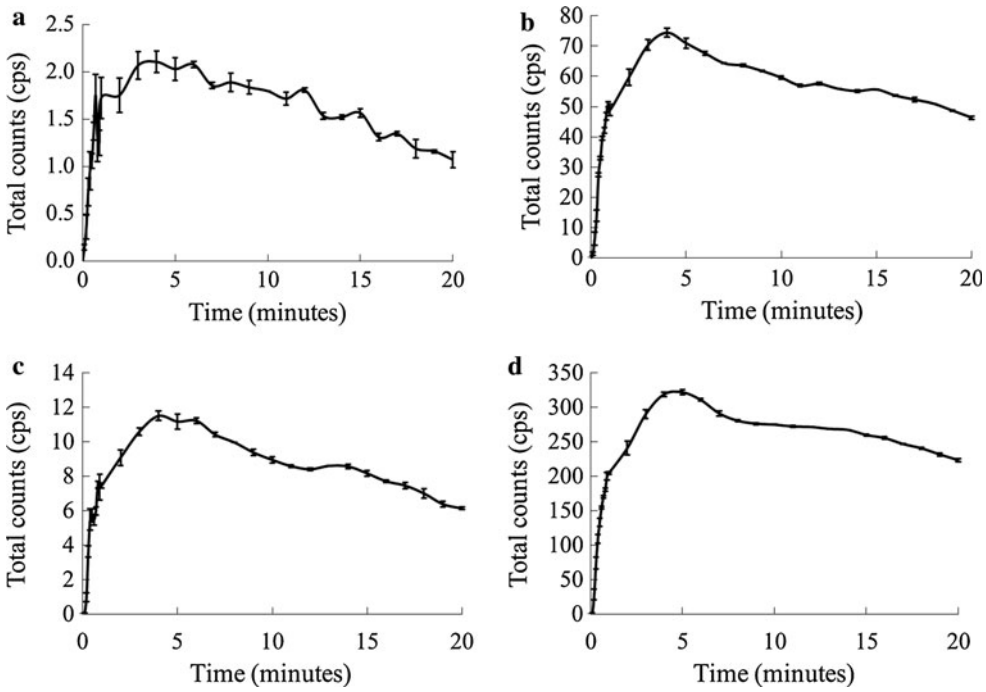

Fig. 4 TACs on planar imaging with ^{99m}Tc-MAG$_3$ using mice. Dynamic data consisted of 108 frames, 2 s/frame for 1 min, 5 s/frame for 4 min and 30 s/frame for 15 min. When using 15 MBq ^{99m}Tc-MAG$_3$, TACs with PAH (**b**) were good, while those with SPH showed no radioactive peaks and large standard deviation (**a**). When 74 MBq ^{99m}Tc-MAG$_3$ was injected into mice, TACs with SPH (**c**) and PAH (**d**) showed radioactive peaks, followed by clear washout

washout period was not smooth when using SPH (Fig. 4a), while TAC with PAH was ideal, due to the higher sensitivity (Fig. 4b); however, the images were very indistinct (Fig. 3b). Although the ROIs were placed over the whole kidneys to assess renal function, ROIs should be placed on the renal cortices in order to accurately determine renal function using 74 MBq ^{99m}Tc-MAG$_3$ imaging with SPH. Thus, it is important to select the appropriate collimator for planar imaging with small animals. However, there has been little research on collimators for providing high-quality images and quantification on planar imaging of small animals.

On bone scintigraphy with ^{99m}Tc-MDP SPECT imaging, SPH and MPH provided SPECT images with higher resolution when compared with PAH (Fig. 5). The backbone on SPECT images was clearly separated using MPH, due to the higher sensitivity. On the other hand, PAH was not suitable for SPECT imaging, as it yielded SPECT images with low resolution. Although Mok et al. [8] reported that MPH was appropriate for bone scintigraphy using ^{99m}Tc-MDP with about 67 MBq, we expected that SPH would be useful with higher radioactivity because the bone scintigraphy was obtained by SPH using ^{99m}Tc-MDP with about 100 MBq [11] and 185 MBq [13], which are higher radioactivity than in our and Mok's study [8].

Although the PAH is often used in clinical imaging, PH should be used to obtain high resolution images on small animal imaging. On planar imaging with our scanner, SPH and PAH could be used, and SPH yielded high-quality images. However, PAH should be used for planar imaging in order to monitor radiopharmacokinetics on whole body imaging with radiotracers having low radioactivity. In addition, PH was suitable for SPECT imaging using our scanner. With PH, we should select SPH, as it yields

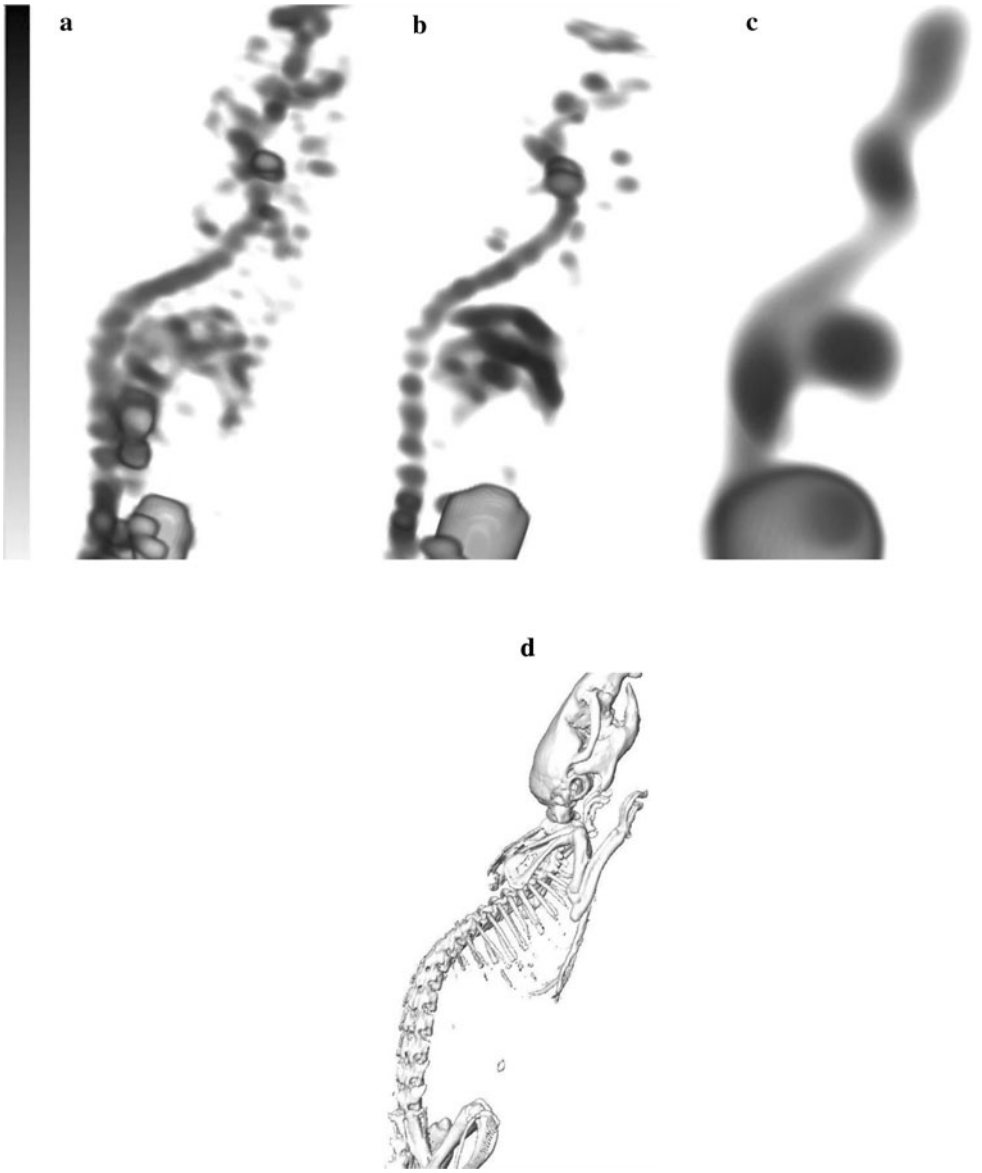

Fig. 5 SPECT images of ^{99m}Tc-MDP using mice. ^{99m}Tc-MDP (74 MBq) was injected into mice, and images were acquired using SPH (**a**), MPH (**b**) and PAH (**c**) for 30 min at 30 min after administration. The CT image was displayed using same slices as the SPECT images (**d**). On ^{99m}Tc-MDP images, MPH showed significant separation of the backbone

high-resolution images, or MPH, as it has higher sensitivity than SPH, depending on the gamma-emitting radionuclide and radioactivity of radiotracers used. This study offered insights into the use of collimators for small animal imaging. Although we should use the same reconstruction method to compare performance of each collimator in the SPECT imaging, the same reconstruction method could not be set up in our scanner. In other scanners, researchers should confirm whether the differences of the reconstruction methods are affected to select the collimators. In addition, the most appropriate collimator will vary depending on scanner, gamma-emitting radionuclide, radioactivity of radiotracers, pharmacokinetics, small animal and/or imaging acquisition method, etc. Based on our results, we have to consider design of collimators to obtain higher quality images.

In conclusion, the characteristics of PH and PAH were different on small animal imaging. Although sensitivity was higher with PAH, PH showed higher resolution. Among the PH collimators, SPH was more appropriate for planar imaging, and MPH was more suitable for SPECT imaging in a small animal scanner with CZT detector.

Acknowledgments The author would like to thank the staff of Chiba University for their technical assistance. This study was partly funded by a Grant-in-Aid for Scientific Research from Japan Society

for the Promotion of Science (23659578, 23659579, 24601008, and 24659558).

References

1. Weisenberger AG, Wojcik R, Bradley EL, Brewer P, Majewski S, Qian J, et al. SPECT-CT system for small animal imaging. IEEE Trans Nucl Sci. 2003;1:74–9.
2. Franc BL, Acton PD, Mari C, Hasegawa BH. Small-animal SPECT and SPECT/CT: important tools for preclinical investigation. J Nucl Med. 2008;49:1651–63.
3. de Kemp RA, Epstein FH, Catana C, Tsui BM, Ritman EL. Small-animal molecular imaging methods. J Nucl Med. 2010; 51:18S–32S.
4. Mueller B, O'Connor MK, Blevis I, Rhodes DJ, Smith R, Collins DA, et al. Evaluation of a small cadmium zinc telluride detector for scintimammography. J Nucl Med. 2003;44:602–9.
5. Funk T, Parnham KB, Patt BE, Li J, Iwanczyk JS, Iwata K. A new CdZnTe-based gamma camera for high resolution pinhole SPECT. Conf Record IEEE Nucl Sci Symp Med Imag. 2003;4:2320–4.
6. Kim H, Furenlid LR, Crawford MJ, Wilson DW, Barber HB, Peterson TE, et al. SemiSPECT: a small-animal single-photon emission computed tomography (SPECT) imager based on eight cadmium zinc telluride (CZT) detector arrays. Med Phys. 2006; 33:465–74.
7. Scheiber C. CdTe and CdZnTe detectors in nuclear medicine. Nucl Instr Meth Phys Res A. 2010;448:513–24.
8. Mok GS, Yu J, Du Y, Wang Y, Tsui Bm. Evaluation of a multi-pinhole collimator for imaging small animals with different sizes. Mol Imag Biol. 2012;14:60–9.
9. Beekman FJ, van der Have F, Vastenhouw B, van der Linden AJ, van Rijk PP, Burbach JP, et al. U-SPECT-I: a novel system for submillimeter-resolution tomography with radiolabeled molecules in mice. J Nucl Med. 2005;46:1194–200.
10. van der Have F, Vastenhouw B, Ramakers RM, Branderhorst W, Krah JO, Ji C, et al. U-SPECT-II: An ultra-high-resolution device for molecular small-animal imaging. J Nucl Med. 2009; 50:599–605.
11. Umeda IO, Tani K, Tsuda K, Kobayashi M, Ogata M, Kimura S, et al. High resolution SPECT imaging for visualization of intratumoral heterogeneity using a SPECT/CT scanner dedicated for small animal imaging. Ann Nucl Med. 2012;1:67–76.
12. Magota K, Kubo N, Kuge Y, Nishijima K, Zhao S, Tamaki N. Performance characterization of the Inveon preclinical small-animal PET/SPECT/CT system for multimodality imaging. Eur J Nucl Med Mol Imaging. 2011;38:742–52.
13. Weber DA, Ivanovic M, Franceschi D, Strand SE, Eriandsson K, Franceschi M, et al. Pinhole SPECT: an approach to in vivo high resolution SPECT imaging in small laboratory animals. J Nucl Med. 1994;35:342–8.
14. Song TY, Choi Y, Chung YH, Jung JH, Min BJ, Hong KJ, et al. Performance amelioration for small animal SPECT using optimized pinhole collimator and image correction technique. IEEE Trans Nucl Sci. 2004;6:3458–62.
15. Qian J, Bradley EL, Majewski S, Popov V, Saha MS, Smith MF, et al. A small-animal imaging system capable of multipinhole circular/helical SPECT and parallel-hole SPECT. Nucl Instr Meth Phys Res A. 2008;594:102–10.
16. Zingermana Y, Golan H, Gersten A, Moalem A. A compact CT/SPECT system for small-object imaging. Nucl Instr Meth Phys Res A. 2008;584:135–48.
17. Figueroa SD, Winkelmann CT, Volkert WA, Hoffman TJ. Performance characteristics of an integrated small animal SPECT/CT unit. Conf Record IEEE Nucl Sci Symp Med Imag. 2005;1752–6.
18. Herrler T, Wang H, Tischer A, Bartenstein P, Jauch KW, Guba M, et al. ^{99m}Tc-MAG3 scintigraphy for the longitudinal follow-up of kidney function in a mouse model of renal ischemia-reperfusion injury. EJNMMI Res. 2012;2:2.
19. Roberts J, Chen B, Curtis LM, Agarwal A, Sanders PW, Zinn KR. Detection of early changes in renal function using ^{99m}Tc-MAG3 imaging in a murine model of ischemia-reperfusion injury. Am J Physiol Renal Physiol. 2007;293:F1408–12.
20. Arveschoug AK, Bertelsen H, Vammen B. Presurgical localization of abnormal parathyroid glands using a single injection of Tc-99m sestamibi: comparison of high-resolution parallel-hole and pinhole collimators, and interobserver and intraobserver variation. Clin Nucl Med. 2002;27:249–54.